Optics Letters

Large-area optical metasurface fabrication using nanostencil lithography

Peter Su,[1,*] Mikhail Shalaginov,[1] Tian Gu,[1,2] Sensong An,[3] Duanhui Li,[1] Lan Li,[1,4,5] Helena Jiang,[1] Seoyoung Joo,[1] Lionel Kimerling,[1] Hualiang Zhang,[3] Juejun Hu,[1,2] and Anuradha Agarwal[1,2]

[1]Department of Materials Science and Engineering, Massachusetts Institute of Technology, Cambridge, Massachusetts 02139, USA
[2]Materials Research Laboratory, Massachusetts Institute of Technology, Cambridge, Massachusetts 02139, USA
[3]Department of Electrical and Computer Engineering, University of Massachusetts Lowell, Lowell, Massachusetts 01854, USA
[4]Currently with Key Laboratory of 3D Micro/Nano Fabrication and Characterization of Zhejiang Province, School of Engineering, Westlake University, 18 Shilongshan Road, Hangzhou 310024, China
[5]Currently with Institute of Advanced Technology, Westlake Institute for Advanced Study, 18 Shilongshan Road, Hangzhou 310024, China
*Corresponding author: peterxsu@mit.edu

Received 15 March 2021; revised 12 April 2021; accepted 16 April 2021; posted 16 April 2021 (Doc. ID 424535); published 5 May 2021

We demonstrate a large-area fabrication process for optical metasurfaces utilizing reusable SiN on Si nanostencils. To improve the yield of the nanostencil fabrication, we partially etch the front-side SiN layer to transfer the metasurface pattern from the resist to the nanostencil membrane, preserving the integrity of the membrane during the subsequent potassium hydroxide etch. To enhance the reliability and resolution of metasurface fabrication using the nanostencil, we spin coat a sacrificial layer of resist to precisely determine the gap between the nanostencil and the metasurface substrate for the subsequent liftoff. 1.5 mm diameter PbTe meta-lenses on CaF_2 fabricated using nanostencils show diffraction-limited focusing and focusing efficiencies of 42% for a 2 mm focal length lens and 53% for a 4 mm focal length lens. The nanostencils can also be cleaned using chemical cleaning methods for reuse.

https://doi.org/10.1364/OL.424535

Optical metasurfaces promise optical components with on-demand control of light and reduced size, weight, and power compared to their bulk counterparts [1–9]. However, fabrication of metasurfaces in the optical spectral range often relies on electron beam lithography due to the high-resolution requirements, which makes fabrication scale poorly with the device dimensions. Recently, deep ultraviolet (DUV) lithography has been validated as a scalable manufacturing route for optical metasurfaces [10–12]. However, DUV lithographic fabrication requires significant capital investment and is limited to standard materials and processes available in foundries.

Here we introduce nanostencil lithography as an alternative technique for scalable, versatile, and rapid prototyping of metasurface devices. Nanostencils are nano-scale shadow masks, which allow repeated fabrication of a pattern via any anisotropic deposition process once the nanostencil is made. Nanostencils have been previously used to fabricate complex oxide nanostructures [13], nanomechanical mass sensors [14], plasmonic nanoantenna arrays [15–17], and biomolecule nanopatterns [18]. All these applications required only deposition of very thin layers (100 nm or less) through the nanostencil, while transmissive dielectric metasurfaces require significantly thicker layers, especially as the wavelength of light increases. They also were limited to nanostencils up to 1 mm by 1 mm in size. In this Letter, we adapt the nanostencil approach to metasurface fabrication and introduce process innovations both in the fabrication of the nanostencils to improve the yield and in the use of the nanostencils to enable reliable and repeatable fabrication of large-area metasurfaces.

The nanostencils were fabricated using the process that is outlined in Fig. 1(a). Starting with a double-sided polished silicon wafer, a 400 nm thick silicon nitride (SiN) layer was grown on both sides using low pressure chemical vapor deposition in a vertical thermal reactor (SVG Thermco VTR 7000). Backside windows for the potassium hydroxide (KOH) etch were subsequently patterned using direct write photolithography (MLA-150, Heidelberg Instruments), followed by reactive ion etching (RIE, LAM 590, Lam Research) of the SiN. Using the

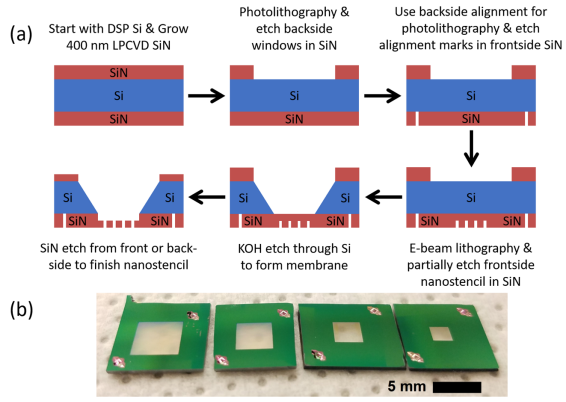

Fig. 1. (a) Schematic of the fabrication process for large-area SiN-based nanostencils. (b) Picture of finished nanostencils ranging in size from 2 mm by 2 mm to 5 mm by 5 mm.

back-side alignment capabilities of the MLA-150, alignment marks were patterned on the front side of the wafer and transferred to the SiN using RIE. These alignment marks were used to align the metasurface pattern defined on the front side using electron beam lithography to the back side window originally patterned on the wafer. The metasurface pattern was transferred to the SiN layer via a partial etch using RIE. A KOH wet etch was used to etch through the silicon wafer and release the SiN membrane carrying the metasurface pattern. Finally, the rest of the SiN membrane was etched through, from either the front or back side, using ECR RIE (Plasmaquest Series II Model 145). This process successfully produced nanostencils up to 5 mm by 5 mm in size, as shown in Fig. 1(b). All stencils showed the same high quality, with no sign of damage under an optical microscope. The dimensions of the membranes and nanostencils can likely be further increased using our method.

This process makes important improvements compared to the processes used in previous nanostencil work [15,19–21]. Unlike the processes used by Kolbel *et al.* [19], van den Boogaart *et al.* [20], and Park *et al.* [21], we did not completely etch through the front-side SiN layer when transferring the metasurface pattern. This helped preserve the integrity of the SiN membrane during the KOH etch, as shown in Fig. 2. The KOH etch only occurs from the back side and is stopped at a blanket SiN layer, instead of etching from both sides and stopping at a SiN membrane with holes, dramatically improving the yield of the nanostencils. The yield was also improved by using methanol, which has a very low surface tension, as the final cleaning agent when cleaning the nanostencil after the KOH etch. Aksu *et al.* [15] avoided the problem of the KOH etch damaging a patterned SiN membrane by patterning the nanostencil after the KOH etch. However, this requires wasting the center area of the wafer such that a vacuum chuck could hold the wafer in place to spin coat electron beam resist for patterning. Our process allows the full area of the wafer to be used, since the KOH etch step occurs after all spin coating steps.

To use our nanostencils, we adapted techniques used previously by Kolbel *et al.* [19,22] and Jain *et al.* [23] and created a new process outlined in Fig. 3(a). Like Kolbel and Jain, we spin coated resist (SPR700) onto the substrate to act as a precise spacer layer between the nanostencil and substrate. This spacer layer was required because the dielectric metasurfaces we fabricated with our nanostencils needed meta-atoms significantly thicker than the nanostencil membrane. Therefore, the photoresist thickness needed to be thick enough to accommodate the desired meta-atom thickness for liftoff, while not being too thick as to cause strong blurring effects [24,25]. We targeted a

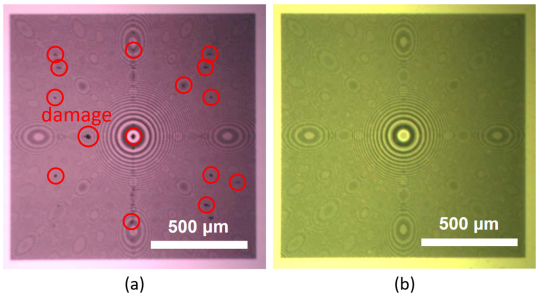

Fig. 2. Optical microscope images of nanostencils after the KOH etch for nanostencils that underwent (a) a complete and (b) a partial etch of the SiN when transferring the metasurface pattern. A complete etch consistently resulted in damage to the nanostencil, circled in red.

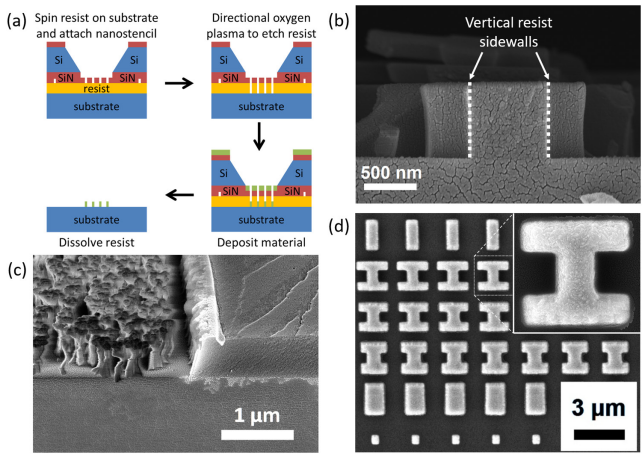

Fig. 3. (a) Schematic of the process for using nanostencils on rigid substrates. (b) SEM image of the resist profile after an anisotropic oxygen plasma etch using an ECR reactive ion etcher, showing the vertical resist profile. (c) SEM image of the resist after an anisotropic oxygen plasma etch using an inductively coupled plasma reactive ion etcher, showing the poor resist etch. (d) SEM image of PbTe meta-atoms deposited using the nanostencil process, showing the clear definition of the edges of the meta-atoms.

750 nm thick spacer layer for our 650 nm thick metasurfaces, but the spacer layer thickness could be easily adjusted by changing the spin coating parameters or the resist. However, unlike Kolbel, we did not pattern the spacer layer into a ring, so when the nanostencil was laid on top and gently pressed onto the resist, van der Waals forces strongly adhered the nanostencil to the resist. This helped ensure an accurate and uniform distance between the nanostencil and the substrate, regardless of the size of the nanostencil membrane. Note that because the resist is used only as a physical spacer, its exposure behavior is not relevant, so the resist can be used without heating it, letting the resist solvent evaporate naturally or by placing the sample under vacuum. Elimination of the heating step can be important if the sample is heat sensitive.

Anisotropic oxygen plasma etching of the resist spacer was performed using an electron–cyclotron resonance (ECR) RIE tool (Plasmaquest Series II Model 145) with 50 sccm of oxygen gas flow at 7 mTorr of pressure, 50 W of ECR power, and 20 W of RF sample bias power. Anisotropic etching was required because the meta-atoms are relatively close to each other, and isotropic etching would create large undercuts and remove the resist supporting the membrane. This could change the spacing between the membrane and the substrate, especially for large membranes. A scanning electron microscopy (SEM) image of the resulting resist profile is shown in Fig. 3(b). The oxygen plasma etch results in vertical sidewalls with a small undercut, similar to that achieved by a double-layer resist liftoff process, although here the nanostencil membrane acts as the top resist. The use of an ECR reactive ion etch is critical. Many different oxygen etch parameters were tried in inductively coupled plasma reactive ion etch tools, with a representative result shown in Fig. 3(c), where the etch leaves a forest of wispy resist behind. This difference can be attributed to the ECR plasma being generated far away from the sample, limiting bombardment of the resist.

The dielectric material, PbTe, is then deposited through the nanostencil apertures, and the nanostencil is lifted off by dissolving the resist in acetone, leaving behind the desired meta-atom pattern, as shown in Fig. 3(d). It should be noted that this process is both substrate-agnostic and meta-atom-material-agnostic, as long as resist can be successfully spin coated on the substrate, and the meta-atom material can be lifted off.

To prove that this nanostencil-based fabrication method produces high-quality metasurfaces and behaves similarly to a double-layer electron-beam resist liftoff process, we used 2 mm by 2 mm nanostencils to fabricate 650 nm thick PbTe dielectric metasurfaces on a CaF_2 substrate. In particular, we demonstrate aspheric meta-lenses with focal lengths of 2 and 4 mm using the same meta-atom geometries previously designed by Zhang *et al.* [26] for operation at a wavelength of 5.2 μm. The designs have a minimum feature size of 400 nm. 1.5 mm diameter tin apertures were patterned on top of the meta-lenses using photolithography. The focal spot quality and optical efficiency were measured using the same protocols adopted by Zhang *et al.* The optical performance of the meta-lenses was compared to ideal lenses with the same diameter and focal lengths. Figure 4 shows the simulated and measured intensity maps at the focal planes, along with the cross sections in both x and y directions. The measured focal spots closely match the simulations, with the measured full-width at half-maximum of 7.56 and 15.5 μm being close to the ideal values of 7.54 and 14.5 μm, showing that the deposited metasurface pattern closely matches what was designed. Both meta-lenses have Strehl ratios exceeding 0.97, indicating that these meta-lenses also achieve diffraction-limited focusing. The measured focusing efficiencies are 42% for the 2 mm focal length lens and 53% for the 4 mm focal length lens. Even though these values are somewhat lower than the 75% figure achieved by Zhang *et al.*, they are comparable to efficiencies reported in state-of-the-art large-area dielectric meta-lenses [10,11].

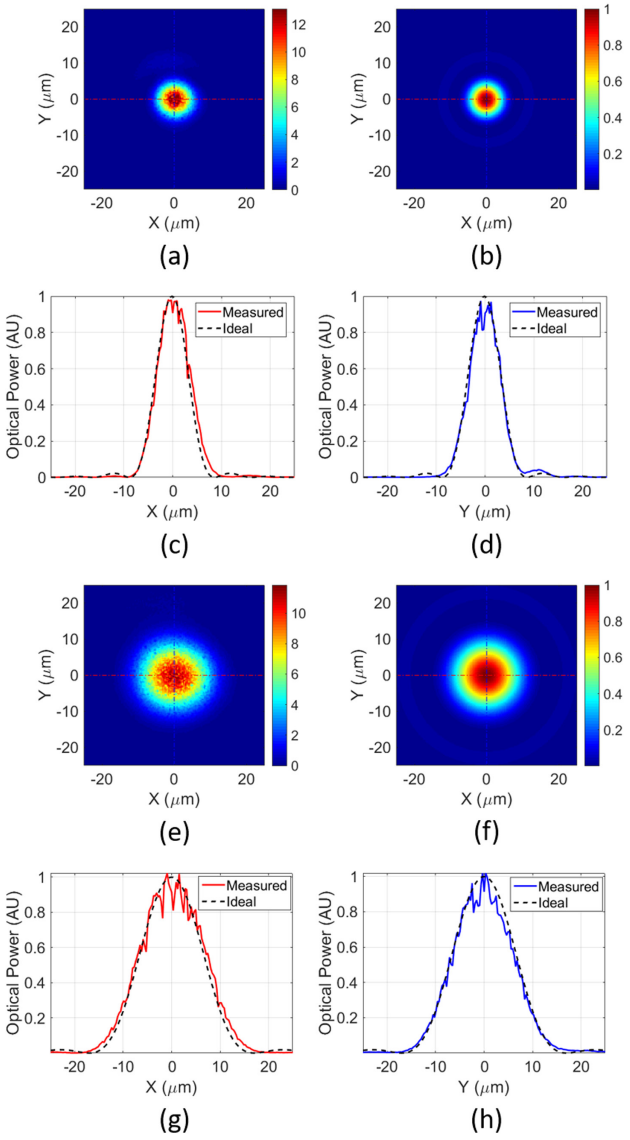

Fig. 4. (a) Measured and (b) simulated focal spot images of the 2 mm focal length meta-lens. The measured focal spot matched the simulation well, as shown by the (c) x-axis and (d) y-axis cross sections. (e)–(h) show the same set of figures for the 4 mm focal length meta-lens.

An important advantage of using nanostencils compared to using a standard lithographic liftoff method is that nanostencils are reusable and therefore do not require repeated lithography to create the same pattern. This is particularly important for patterns with small feature sizes that require a serial lithography method such as electron beam lithography. However, the apertures of the nanostencil do gradually clog as materials are deposited through them [25]. Therefore, it is important that the nanostencils can be cleaned, which was previously demonstrated using wet chemical methods to remove deposited metals such as aluminum [27]. Figure 5 shows an optical microscope image of the nanostencil immediately after using it to pattern a PbTe metasurface and then after cleaning the nanostencil by soaking it in a solution of 2 vol% H_2O_2, 48 vol% HBr, and 50 vol% citric acid for 90 s [28]. The nanostencil shows a clear color change due to the removal of the deposited PbTe thin film without compromising the structural integrity of the stencil, ensuring repeatable usages.

In conclusion, we have developed and demonstrated a large-area fabrication process for optical metasurfaces utilizing reusable nanostencils. To improve the yield of the nanostencil fabrication, we utilized a partial etch of the nanostencil pattern into the front-side SiN layer to preserve the integrity of the membrane during the KOH etch. To enhance the reliability and resolution of the use of the nanostencil, we utilized a sacrificial layer of resist to precisely determine the gap between the nanostencil and the substrate. This process demonstrates repeatability matching that of standard liftoff techniques for meta-lenses with 400 nm minimum feature sizes. The nanostencils can also be

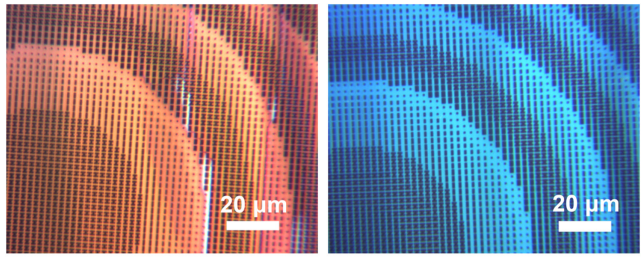

Fig. 5. Optical microscope images of a nanostencil (a) after deposition of PbTe and liftoff and (b) after chemical cleaning using a solution of 2 vol% H_2O_2, 48 vol% HBr, and 50 vol% citric acid [28].

cleaned using chemical cleaning methods for reuse. It is expected that this fabrication process can produce metasurfaces with feature sizes below 100 nm due to the resolution capabilities of electron beam lithography [18,23].

Funding. Defense Advanced Research Projects Agency (HR00111720029).

Acknowledgment. The authors would like to acknowledge the staff and facilities provided by the Massachusetts Institute of Technology (MIT) Materials Research Laboratory and Fab.nano.

Disclosures. The authors declare no conflicts of interest.

Data Availability. Data underlying the results presented in this paper are not publicly available at this time but may be obtained from the authors upon reasonable request.

REFERENCES

1. A. V. Kildishev, A. Boltasseva, and V. M. Shalaev, Science **339**, 1232009 (2013).
2. S. B. Glybovski, S. A. Tretyakov, P. A. Belov, Y. S. Kivshar, and C. R. Simovski, Phys. Rep. **634**, 1 (2016).
3. P. Genevet, F. Capasso, F. Aieta, M. Khorasaninejad, and R. Devlin, Optica **4**, 139 (2017).
4. S. M. Kamali, E. Arbabi, A. Arbabi, and A. Faraon, Nanophotonics **7**, 1041 (2018).
5. A. Zhan, S. Colburn, C. M. Dodson, and A. Majumdar, Sci. Rep. **7**, 1673 (2017).
6. M. Y. Shalaginov, S. D. Campbell, S. An, Y. Zhang, C. Ríos, E. B. Whiting, Y. Wu, L. Kang, B. Zheng, C. Fowler, H. Zhang, D. H. Werner, J. Hu, and T. Gu, Nanophotonics **9**, 3505 (2020).
7. D. Lin, P. Fan, E. Hasman, and M. L. Brongersma, Science **345**, 298 (2014).
8. Y. Zhou, I. I. Kravchenko, H. Wang, J. R. Nolen, G. Gu, and J. Valentine, Nano Lett. **18**, 7529 (2018).
9. M. Y. Shalaginov, S. An, F. Yang, P. Su, D. Lyzwa, A. M. Agarwal, H. Zhang, J. Hu, and T. Gu, Nano Lett. **20**, 7429 (2020).
10. J. S. Park, S. Zhang, A. She, W. T. Chen, P. Lin, K. M. A. Yousef, J. X. Cheng, and F. Capasso, Nano Lett. **19**, 8673 (2019).
11. T. Hu, Q. Zhong, N. Li, Y. Dong, Z. Xu, Y. H. Fu, D. Li, V. Bliznetsov, Y. Zhou, K. H. Lai, Q. Lin, S. Zhu, and N. Singh, Nanophotonics **9**, 823 (2020).
12. A. She, S. Zhang, S. Shian, D. R. Clarke, and F. Capasso, Opt. Express **26**, 1573 (2018).
13. C. V. Cojocaru, C. Harnagea, F. Rosei, A. Pignolet, M. A. F. Van Den Boogaart, and J. Brugger, Appl. Phys. Lett. **86**, 183107 (2005).
14. J. Arcamone, M. A. F. Van Den Boogaart, F. Serra-Graells, J. Fraxedas, J. Brugger, and F. Pérez-Murano, Nanotechnology **19**, 305302 (2008).
15. S. Aksu, A. A. Yanik, R. Adato, A. Artar, M. Huang, and H. Altug, Nano Lett. **10**, 2511 (2010).
16. S. Aksu, A. A. Yanik, R. Adato, A. Artar, M. Huang, and H. Altug, Proc. SPIE **8031**, 80312U (2011).
17. S. Aksu, A. E. Cetin, R. Adato, and H. Altug, Adv. Opt. Mater. **1**, 798 (2013).
18. M. Huang, B. C. Galarreta, A. Artar, R. Adato, S. Aksu, and H. Altug, Nano Lett. **12**, 4817 (2012).
19. M. Kölbel, R. W. Tjerkstra, G. Kim, J. Brugger, C. J. M. Van Rijn, W. Nijdam, J. Huskens, and D. N. Reinhoudt, Adv. Funct. Mater. **13**, 219 (2003).
20. M. A. F. Van Den Boogaart, G. M. Kim, R. Pellens, J. P. Van Den Heuvel, and J. Brugger, J. Vac. Sci. Technol. B **22**, 3174 (2004).
21. C. W. Park, O. Vazquez Mena, M. A. F. Van Den Boogaart, and J. Brugger, J. Vac. Sci. Technol. B **24**, 2772 (2006).
22. M. Kölbel, R. W. Tjerkstra, J. Brugger, C. J. M. Van Rijn, W. Nijdam, J. Huskens, and D. N. Reinhoudt, Nano Lett. **2**, 1339 (2002).
23. T. Jain, M. Aernecke, V. Liberman, and R. Karnik, Appl. Phys. Lett. **104**, 083117 (2014).
24. O. Vazquez-Mena, L. G. Villanueva, V. Savu, K. Sidler, P. Langlet, and J. Brugger, Nanotechnology **20**, 415303 (2009).
25. M. Lishchynska, V. Bourenkov, M. A. F. van den Boogaart, L. Doeswijk, J. Brugger, and J. C. Greer, Microelectron. Eng. **84**, 42 (2007).
26. L. Zhang, J. Ding, H. Zheng, S. An, H. Lin, B. Zheng, Q. Du, G. Yin, J. Michon, Y. Zhang, Z. Fang, M. Y. Shalaginov, L. Deng, T. Gu, H. Zhang, and J. Hu, Nat. Commun. **9**, 1481 (2018).
27. O. Vázquez-Mena, G. Villanueva, M. A. F. van den Boogaart, V. Savu, and J. Brugger, Microelectron. Eng. **85**, 1237 (2008).
28. G. P. Malanych, V. N. Tomashyk, I. B. Stratiychuk, and Z. F. Tomashyk, Inorg. Mater. **52**, 106 (2016).